



### **Science Arts & Métiers (SAM)**

is an open access repository that collects the work of Arts et Métiers Institute of Technology researchers and makes it freely available over the web where possible.

This is an author-deposited version published in: <https://sam.ensam.eu>  
Handle ID: <http://hdl.handle.net/10985/14435>

#### **To cite this version :**

Mario RENDEROS, Amaia TORREGARAY, Esther GUTIERREZ-ORRANTIA, Franck GIROT, Nicolas SAINTIER - Microstructure characterization of recycled IN718 powder and resulting laser clad material - Materials Characterization n°134, p.103-113 - 2017

Any correspondence concerning this service should be sent to the repository

Administrator : [scienceouverte@ensam.eu](mailto:scienceouverte@ensam.eu)





### **Science Arts & Métiers (SAM)**

is an open access repository that collects the work of Arts et Métiers ParisTech researchers and makes it freely available over the web where possible.

This is an author-deposited version published in: <https://sam.ensam.eu>  
Handle ID: <http://hdl.handle.net/null>

#### **To cite this version :**

Nicolas SAINTIER, Nicolas SAINTIER - Microstructure characterization of recycled IN718 powder and resulting laser clad material - Materials Characterization SCIENCE DIRECT n°134, p.103-113 - 2017

# Microstructure characterization of recycled IN718 powder and resulting laser clad material



Mario Renderos<sup>a</sup>, Amaia Torregaray<sup>a</sup>, M<sup>a</sup>. Esther Gutierrez-Orrantia<sup>a</sup>, Aitzol Lamikiz<sup>a</sup>,  
Nicolas Saintier<sup>b</sup>, Franck Giroit<sup>a,c,\*</sup>

<sup>a</sup> University of the Basque Country, UPV/EHU, Faculty of Engineering, Alameda de Urquijo s/n, 48013 Bilbao, Bizkaia, Spain

<sup>b</sup> I2M, Université de Bordeaux, Arts et Métiers ParisTech, Esplanade Arts et Métiers, 33400 Talence, France

<sup>c</sup> IKERBASQUE, Basque Foundation for Science, Bilbao, Spain

## ARTICLE INFO

### Keywords:

Laser Material Deposition  
IN718 powder recycling  
EBSD  
EDX  
Mechanical characterization

## ABSTRACT

The possibility to reuse the metal powder wasted in Laser Material Deposition (LMD) process has been evaluated and a simple procedure developed. LMD uses metal powder which is fed through a nozzle into the focal point of a laser, where it melts the powder and the substrate material. During the process, a high ratio of particles hits against an unmelted area and directly bounces off the deposited area. The efficiency ratio of deposition can drop to 40% depending on the configuration and spot size. This work deals with the design of a procedure to recollect and reuse the wasted powder of a nickel based superalloy IN718. After usage, powder is recollect, undesired fractions are magnetically segregated and aggregates are removed by sieving. The particles are mixed again and ready for reuse. In order to study the effectiveness of the process, no new powder has been added to the recovered fraction, and this procedure has been repeated five times. Experimental tests show that deposited material present similar properties than those obtained with new powder grains. But, after 3 reuses, the porosity content increases consequently and the rupture strain decreases strongly. The implementation of this process allows the improvement of the final efficiency, reducing costs and decreasing the hazardous powder amount.

## 1. Introduction

Additive Manufacturing processes (AM), and Laser Material Deposition (LMD) process in particular, are becoming an important alternative for manufacturing metallic complex structures and high added value part repairs. Main applications of LMD are turbine blade repair, hard coatings for complex tools for mining and oil industry and manufacturing of complex structures onto a previously manufactured substrate. Main benefits of the process are the drastic reduction of wasted material since LMD process is a Near-Net Shape process. Furthermore a very low amount of chips and scraps is generated. The process is based on the injection of a metallic material into a previously melted pool of substrate material. The surface of the part where the material is being deposited is melted by a laser and an external material (usually a powder stream) is deposited and melted together with the base material [1]. The most common configuration of the process is based on using a coaxial nozzle to inject powder coaxially to the laser (Fig. 1).

One of the main drawbacks of the process is the trapped powder efficiency. The powder needs to be injected into the melt pool but a

high ratio of the particles hits against unmelted area and directly bounces off the deposited area. The efficiency ratio of trapped particles can drop to 40% depending on the configuration of the nozzle and the laser spot size [2]. Therefore, a relatively high waste of metallic particles is generated. A large part of these particles was not damaged and can be reused. On the other hand, the rest of the particles is heat affected and may (i) be partially oxidized, (ii) be partially melted and/or (iii) undergo variations of its chemical composition.

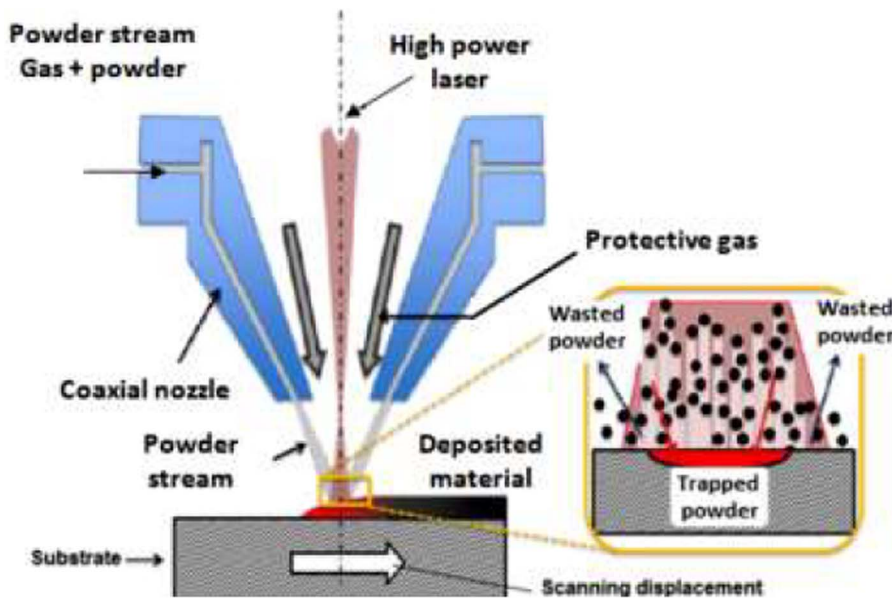
Research has been mainly focused on the parameters of the process, like overlap distance [3–5], laser power and/or feed rate [6] or the metallurgical properties of the manufactured components [7]. Few studies have been carried out to assess how recycling particles after high power laser manufacturing process affect the component properties and behavior. Taken into account the specific characteristics that metallic powder used in LMD process should provide (as spherical shape or plane grain surface), the cost of the powder is higher than other raw geometries as wire or sheet (usually three or four times higher than cast material).

In the last years, researchers were interested by powder recyclability in Selective Laser Melting (SLM) [8] and Electron Beam Melting

\* Corresponding author at: University of the Basque Country, UPV/EHU, Faculty of Engineering, Alameda de Urquijo s/n, 48013 Bilbao, Bizkaia, Spain.

E-mail addresses: [marioalfredo.renderos@ehu.eus](mailto:marioalfredo.renderos@ehu.eus) (M. Renderos), [amaia.torregaray@ehu.eus](mailto:amaia.torregaray@ehu.eus) (A. Torregaray), [esther.gutierrez@ehu.eus](mailto:esther.gutierrez@ehu.eus) (M.E. Gutierrez-Orrantia), [aitzol.lamikiz@ehu.eus](mailto:aitzol.lamikiz@ehu.eus) (A. Lamikiz), [nicolas.saintier@ensam.eu](mailto:nicolas.saintier@ensam.eu) (N. Saintier), [frank.giroit@ehu.eus](mailto:frank.giroit@ehu.eus) (F. Giroit).

and detail of trapped and wasted powder.



(EBM) [9,10]. The powder outside the melting area can be recycled. This contributes to economic viability and sustainability of these technologies. In each case, the powder characteristics and chemical composition are critical parameters to ensure repeatable process and suitable mechanical properties of metal components built. To ensure reliable and repeatable fabrication, the controls of powder stock properties as well as the variation limits are necessary. It is also important to understand how high power and high temperature of AM processes affect the recycled powder characteristics.

Strondl et al. [8] have pointed out, in the case of IN718 recycled powder, sieved and blended with 5% of new powder, processed using SLM, (i) no change in particles morphology or composition but disappearance of smaller particles, (ii) oxygen absorption which can explain a slight porosity increase in the manufactured part, (iii) no change in processed microstructure, yield and ultimate tensile strengths and (iv) decrease in ductility and impact toughness likely associated to oxygen absorption.

Petrovic et al. [9] used only sieved Ti6Al4V powder for the EBM process, and concluded that (i) there is no change in powder composition, (ii) large oxygen absorption but hydrogen decreasing (iii) no general morphology change apart from occasional aggregates and (iv) a maximum of 12 cycles for reusing the powder.

Nandwana et al. [10] demonstrated that IN718 powders can sustain a large number of cycles without a change in powder and subsequently build chemistries. There is no significant change in the flowability, morphology, and size distributions of IN718 powders with build cycles. The initial powder chemistries and the alloy system under consideration are the key factors in governing the recyclability in powder bed systems, with oxygen pickup being the limiting factor.

Ardila et al. [11] defined a simple methodology based on sieving and drying of the IN718 powder and pointed out (i) material use efficiency larger than 95%, (ii) stable and sound properties obtained in all test samples irrespective of the iteration number. The IN718 powder morphology does not significantly change during its reuse: most of the particles remained spherical and particle size distribution after several production cycles was similar, with the exception of a small amount of particle aggregates that were detected with sizes between 50 and 100  $\mu\text{m}$ . Material composition remained also unchanged.

LPW Technology [12] analyzed the IN718 powder degradation during the SLM process. The wasted powder is sieved to remove coarse particles generated during the melting process and dried. After 25 builds, there was a significant increase in UTS, reduction in ductility from 20% to 13% and a little increase in oxygen with each reuse.

Carroll et al. [13], presented a methodology to reuse Waspaloy™ powder. The recycling methodology was similar with filtering and drying of the wasted particles. Recycling the powder up to 10 times produces only minor changes in the composition, morphology, surface texture of the powder and in its size distribution.

Slotwinski et al. [14] showed how virgin powder changes after being exposed to and recycled from one or more Direct Metal Laser Sintering (DMLS) additive manufacturing build cycles, in the case of CoCr and 17-4 SS alloys. They pointed out that recycling increases powder size distribution with progressive builds. The stainless steel powder in the sieve residue shows characteristics of melting and particle joining.

Rao et al. [15] studied the behavior of IN 718 powders with varied oxygen levels of 275, 180 and 140 ppm, consolidated by hot isostatic pressing (HIP). Tensile properties of the HIP + heat treated alloys have shown that the yield strength (YS), ultimate tensile strength (UTS) do not get influenced by the oxygen content, but the ductility was found to be deteriorated drastically with increasing the oxygen content of the alloy.

Powder reuse is a hot topic for SLM based processes since powder cost is significantly higher and the amount of wasted powder is also much higher than in the LMD process. Furthermore, the metallic powder is a hazardous and difficult to treat waste. It is also important to consider the typical powder size in LMD process ranges from 45 to 150  $\mu\text{m}$ , and their associated health and safety issues [16].

The objective of this study is to evaluate the recyclability of IN718 metal powder in the laser cladding process, since no data are available for this additive manufacturing process. To show that simple methods such as filtering, magnetic segregation and drying are in fact sufficient to allow powder to be reused. The metallic powders have been reused up to four times and corresponding builds have been manufactured. Each part has been evaluated through metallurgical and mechanical tests in order to evaluate the evolution of the material characteristics with the number of reuses.

## 2. Materials and Methodology

### 2.1. Materials

In this study, an IN718 build has been clad on a substrate material made of DIN C45E steel. The final dimensions of the sample were 18 × 15 × 107 mm. The IN718 metal powder used were an atomized alloy from Oerlikon Metco Company (Metcoclad 718 powder) with

**Table 1**  
Chemical composition of Metcoclاد™ 718 powder.

Element	Al	C	Co	Cr	Cu	Fe	Mn	Mo
Wt%	0.46	0.02	0.02	18.72	0.01	18.18	0.04	2.99
Range	0.20–0.80	0.08 max.	1.00 max.	17.00–21.00	0.30 max	Balance	0.35 max.	2.80–3.30

Element	Nb	Nb + Ta	Ni	P	S	Si	Ta	Ti
Wt%	4.96	4.97	53.6	< 0.01	< 0.01	0.04	0.01	0.80
Range		4.75–5.50	50.00–55.00	0.015 max.	0.015 max.	0.35 max.		0.65–1.15

**Table 2**  
Laser parameters used.

Power (W)	Scanning speed (mm/s)	Powder feed (gr./min)	Spot diameter (mm)	Overlap by track (%)	Offset by layer (%)
571	8.75	8.78	1	26	25

spherical shape and a particle size ranging from 45 to 106  $\mu\text{m}$ . The chemical composition of the material is given in Table 1.

## 2.2. Equipment and Process Parameters

The processing for the different test-builds has been carried out with the following configuration: a cladding cell Aktinos 500 with CNC control equipped with a coaxial LMD nozzle developed by the UPV/EHU University in previous works. A multi-mode Rofin FL 010 diode laser has been incorporated to the nozzle as well as an argon gas flux regulator system for protective and powder driving functions (video of the equipment and the process available at the following address: <https://www.youtube.com/watch?v=FWOVgSVSvjC>). The particles are stored in a hopper where the temperature can be adjusted to remove moisture (60 °C). They are injected into the coaxial LMD nozzle, its mass flow being controlled. In order to collect the wasted powder in a proper way, the laser machine has been equipped with a metallic tray located at the bottom of the substrate surrounded completely to avoid cross contamination. Table 2 shows the values of the parameters used for the manufacturing of the samples (powder feed, scanning speed,

laser power, spot diameter, offset and overlapping). The scanning direction has been kept the same during the building up of the clad builds.

## 2.3. Recycling Procedure and Manufacturing of Test Samples

Visual inspections of the used powder showed the formation of new phases with magnetic properties in a very low fraction. This characteristic has been used to segregate them from the non-deposited and non-reacted metal powder. The production of the test samples and the recycling procedure of the non deposited powder have been carried out following the scheme of Fig. 2.

Once the first test sample has been built with new metal powder, the wasted powder is collected from the tray and an EDX analysis is subsequently carried out. The wasted powder recycling has been done following this procedure.

1. The wasted powder slides first on an inclined magnetic tray (activated electromagnetically or by permanent magnets) which can be vibrated to facilitate the flowing of the particles. The unwanted phases are removed by adhering to the magnetic tray as the rest of the material slides into the sieve. The magnetic tray is cleaned regularly. The separation process can be repeated several times until no particles stick to the magnetic tray.
2. Once the magnetic fraction is removed, the cleaned fraction is sieved in order to check particle size distribution. When the particle size has been measured, all the clean fractions are blended again, trying to respect the Gaussian distribution curve of the initial particle sizes. The sizes of different sieves used meet those of the initial

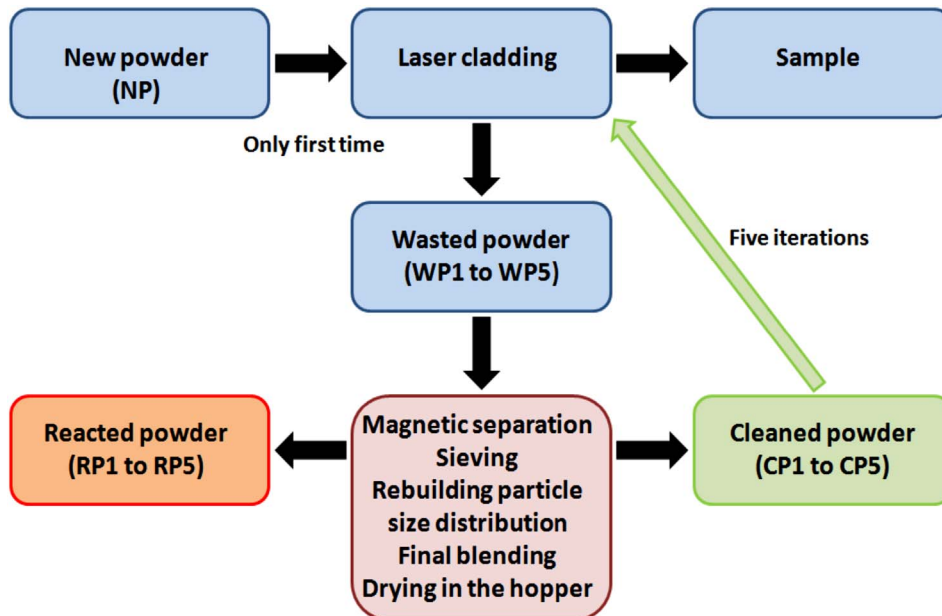


Fig. 2. Scheme of the recycling process.



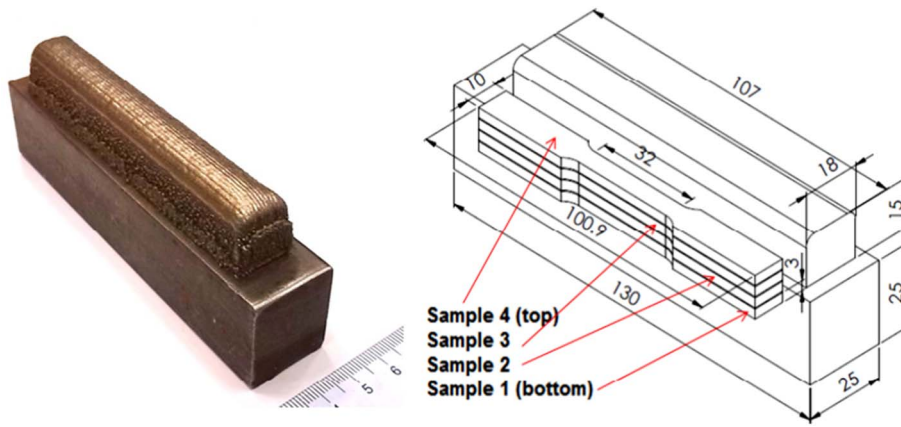


Fig. 3. a) Geometry of the clad part obtained on its steel support; b) test part design and position of the samples within the clad part.

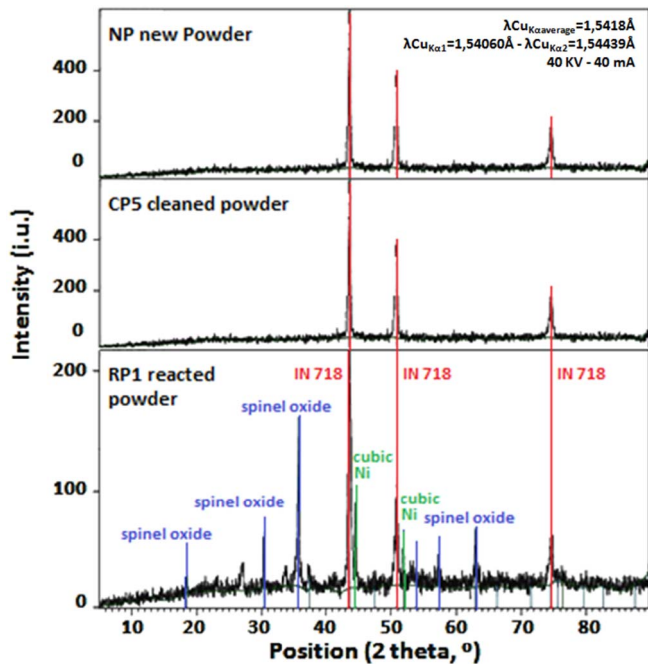


Fig. 4. Diffraction of IN718 powder: NP new powder (top), CP5 cleaned powder (middle) and RP1 reacted powder (bottom).

grain size of the new powder, namely: < 53  $\mu\text{m}$ , 53–63  $\mu\text{m}$ , 63–71  $\mu\text{m}$ , 71–90  $\mu\text{m}$ , 90–105  $\mu\text{m}$ , 105–150  $\mu\text{m}$  and > 150  $\mu\text{m}$ . During the final blending of the clean powder of the *i*th iteration, we

tried to always maintain the same proportion of each different size classes.

3. The cleaned powder was reintroduced in the hopper of the feeder system for manufacturing a new build. New powder is not added and all the used material comes from the recycled powder obtained following the procedure. Drying of the cleaned powder is achieved directly in the hopper.

This procedure has been repeated five times. At the end of each loop, five metallic builds designed to prepare samples for mechanical properties and microstructure observations are obtained. The build is cut from its substrate and heat treated as follows: precipitation hardening, 720 °C during 8 h and 620 °C for 18 h. The tensile samples were then machined by wire EDM. Fig. 3 shows one of the builds built in each recycling loop, as well as the test parts which have been obtained.

### 3. Results and Discussion

#### 3.1. Chemical Analysis

The wasted powder was analyzed by Energy-Dispersive X-ray Spectroscopy (EDX) in order to define the composition of the powder and X-rays Diffraction (XRD) for crystal information and structure using a Jeol JSM-6400 SEM equipment. Spectra obtained from the wasted powder (XRD and EDX) and analyzed by PANalytical Xpert PRO, point out the presence of the base alloy IN718 and a scarce amount of other phases.

There is no difference in the spectra of the NP new powder and those of CP1 and CP5 cleaned powders (Fig. 4). The crystal structure is then the same whatever the number of uses.

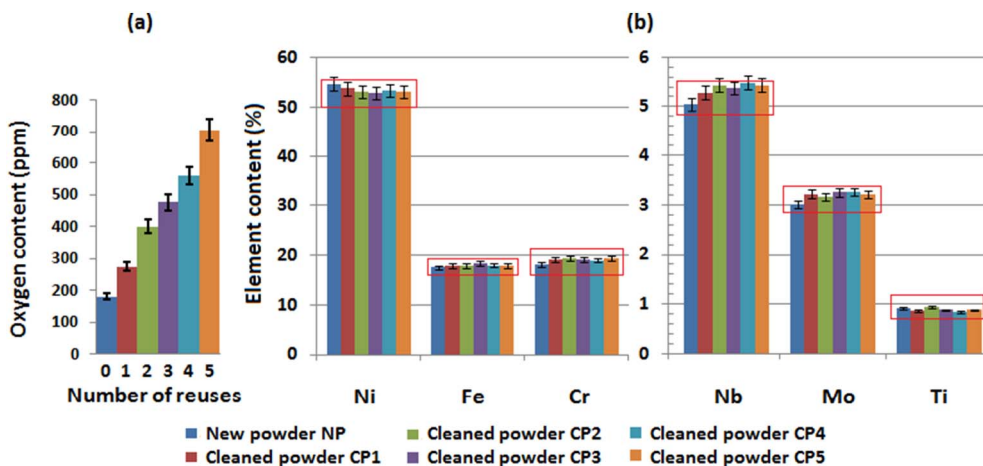


Fig. 5. (a) Oxygen content of the NP new powder and CP1 to CP5 cleaned powders after the different recycles; (b) chemical composition of the NP new powder and CP1 to CP5 clean powders. In red, the compositional requirements range of IN718 (AMS 5662M). (For interpretation of the references to color in this figure legend, the reader is referred to the web version of this article.)

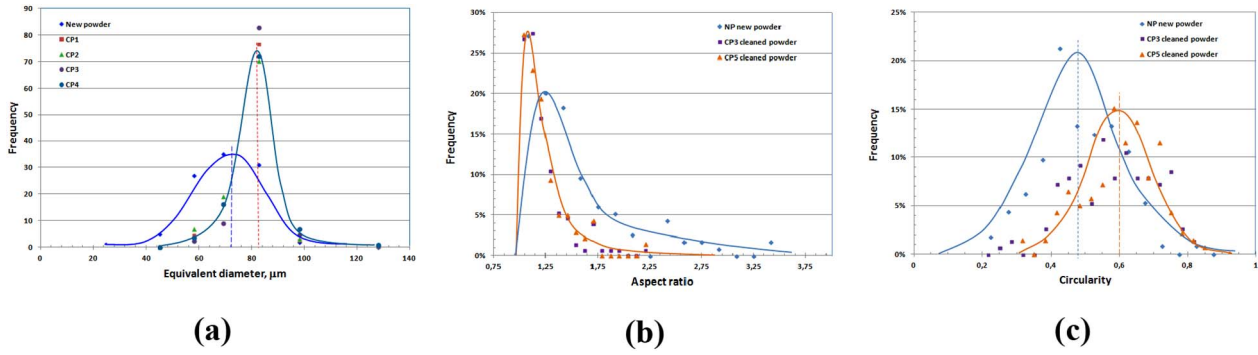


Fig. 6. Distribution curve of grain size (a), circularity (b) and aspect ratio (c) distribution of the NP new powder, CP3 and CP5 cleaned powders obtained after each iteration.

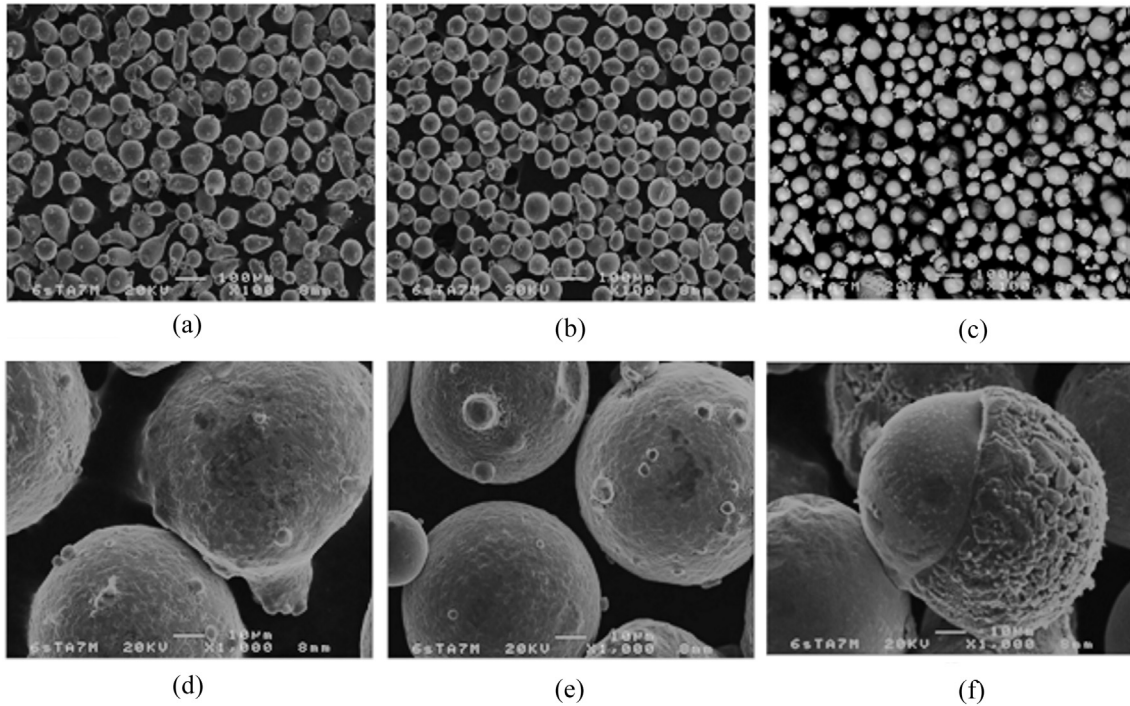


Fig. 7. Scanning Electron Microscope micrographs of the new powder NP (a) and (b), the cleaned powder of the 3th iteration CP3 (c) and (d), Backscattered Scanning Electron Microscope micrographs of the reacted powders RP3 (e) and SEM details of the acorn-shaped particles (red arrows in previous pictures) of spinel oxide cubic phase.

Once magnetic segregation has been done, the spectra obtained from the reacted powder (RP1 to RP5) show the presence of other compounds than the base alloy (Fig. 4). Moreover, it has been seen by XDR that magnetic fraction removed also contains a small amount of IN718 alloy powder (non-magnetic), surely trapped and pushed by the magnetic phase particles in the segregation process.

These phases have been characterized by XRD and they have been identified as IN718 alloy, Ni cubic phase element and spinel type ferrous oxides (hexoctahedral phase such as  $\text{NiFe}_2^{3+}\text{O}_4$  similar to Trevorite). Since all the undesirable detected phases present magnetic properties; this characteristic has been very useful to segregate them from the non-deposited and non-reacted metal powder. The ratio of undesirable phases has been estimated to be  $< 2\%$  by weighting the different fractions.

Oxygen content of the cleaned powder has been measured using a LECO ON736 Oxygen/Nitrogen Elemental Analyzer (Fig. 5a). Although the oxygen content remains quite low, it increases linearly with the number of reuses. This can be explained by a mild oxidation of the particles outside the trapped zone but subjected to the high temperatures of the laser irradiation (particles located near to the thermal affecting zone but bouncing out of it) where the protective gas injected through the clad nozzle is not sufficiently effective. Some authors

[10,12] have also pointed out that recycling increases the oxygen content of the powder with progressive builds (EBM or DMLS).

The chemical composition of cleaned powders has been analyzed after each iteration (Fig. 5b). The variations in chemical composition agree with the extraction of the magnetic phases: nickel and iron percentages slightly decrease (as they are the main components of extracted magnetic phases) and the rest of elements increases, but without changing the chemical composition of the powder significantly. Fig. 5b shows also the ranges (marked with red rectangles) that comply with compositional requirements of IN718 standards (AMS 5662M). All the elements measured have a satisfactory proportion for the 5 iterations realized. Nevertheless, niobium content increases in each loop and therefore it may be concluded that this element could define the limit of the recyclability in terms of chemical composition. Ardila et al. [11] have pointed out a similar evolution of Nb in their recycled powders for SLM.

### 3.2. Powder Grain Size and Morphology

Powder grain size has been measured by sieving the powders at different steps, from new material or zero use up to the fifth use in the cladding process and also by image analysis of SEM pictures of the

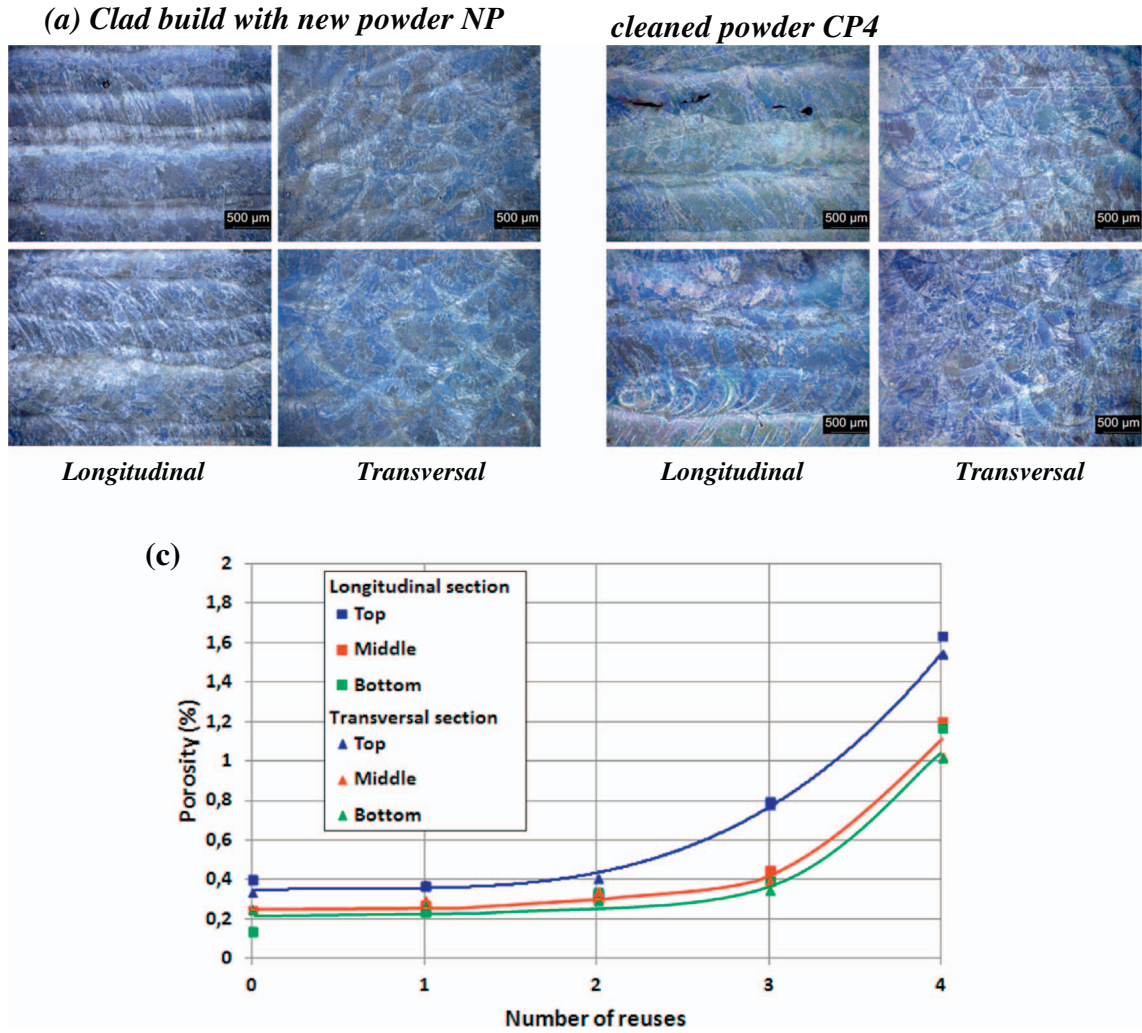


Fig. 8. Optical micrographs of longitudinal section of clad builds (top and bottom parts) with NP powder (a), CP4 powder (b), and evolution of the level of porosity in the clad builds with the number of powder reuses (c).

different new and recycled powders. Fig. 6 shows the distribution curve of the grain size for CP3, CP5 and NP powders. The change in particles size is effective after the first use. It seems that a near steady-state in mean grain size and standard deviation values exist.

This mean size of the powder grains increases from 72  $\mu\text{m}$  for the new powder to 83  $\mu\text{m}$  for the cleaned powders when the standard deviation decreases from 15.5  $\mu\text{m}$  to 12  $\mu\text{m}$ . The recycled particles are a bit larger and more centered around their mean value than the new particles. The cleaned particles present a more homogenous size distribution than the new particles. This effect has been also reported by several authors [8,10,11,13,14] in the case of EBM, SLM, LDMD or DMLS.

SEM observations and their posterior image analysis have pointed out an evolution in the morphology of the cleaned particles with a variation of circularity (Fig. 6b) from 0.48 to 0.60 and of aspect ratio (Fig. 6c) from 1.51 to 1.21, respectively for the new particles and for the clean powders. This means that after recycling the remaining particles are more spherical than the new ones (circularity and aspect ratio reaching the value 1). Backscattered SEM images (Fig. 7) showed at the surface of the particles, dark zones mainly associated to a mild oxidation of the particles surface (Fig. 7b–d). The SEM analysis of the reacted particles (Fig. 7e–f) pointed out the presence of melted or partially melted particles with an acorn-shape made of spinel oxide cubic phase (similar to Trevorite  $\text{NiFe}_2\text{O}_4$ ).

These particles are not present in the cleaned powder which means that the magnetic separation process is effective. Slotwinski et al. [14]

also showed in the case of stainless steel powders in DMLS that the sieve residue had characteristics of melting and particle joining.

### 3.3. Microstructure of Clad Materials

#### 3.3.1. Chemical Composition of the Clad Builds

The chemical composition of the clad build was analyzed by Energy-Dispersive X-ray Spectroscopy (EDX), through the thickness of each clad build. The results show that the contents of the different elements remain the same whatever the position in the clad build (top or bottom part) or the cleaned powder iteration number (new powder or one of the 5th iterations). After 5 iterations, the composition of the clad build remains in the limits of the IN718 standard (AMS 5662M).

#### 3.3.2. Microstructure

The optical micrographs of the clad samples shown in Fig. 8a–b reveal an almost directionally solidified dendritic microstructure. The columnar dendrites are aligned quasi parallel to the build direction. There is no great difference between the samples built with new powder and the recycled powder. These observations are consistent with previous work done on this material [17]. The main difference between the top and the bottom of the build is the presence of some porosity. The porosity content seems to be higher in the top of the build than in the bottom whatever the number of reuses, and higher for the cleaned powder CP4 than for the new powder NP. Porosity has then been



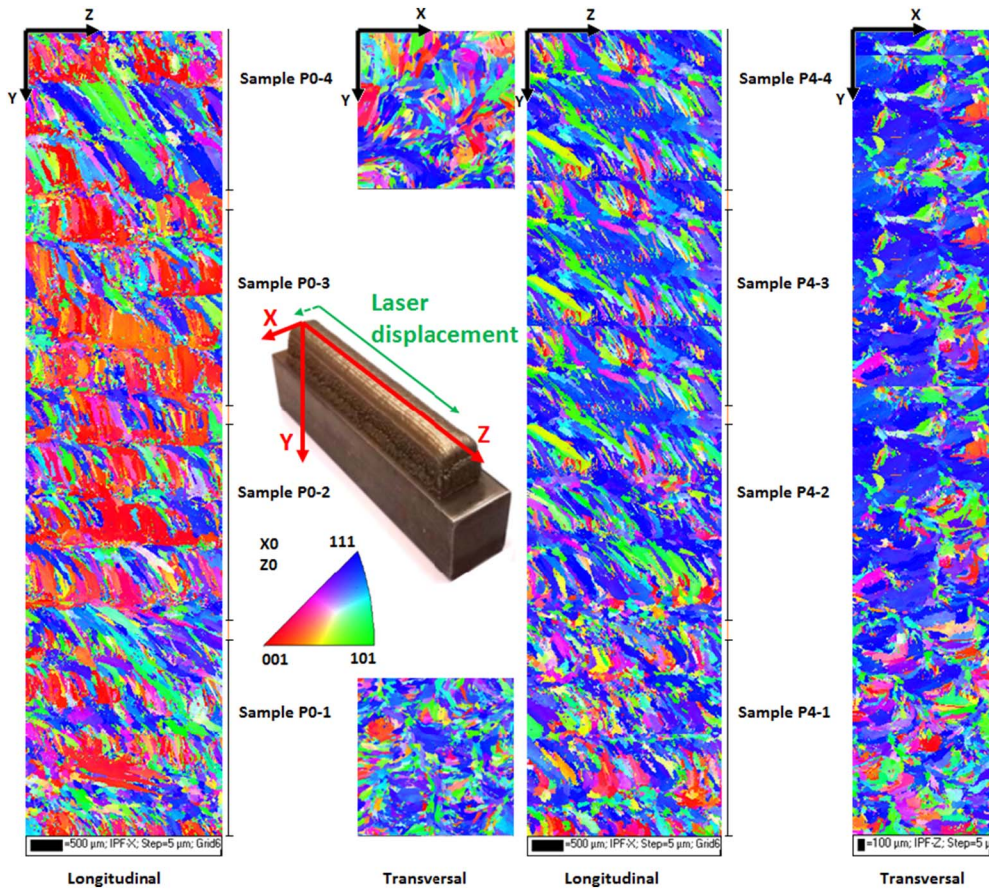


Fig. 9. EBSD analysis of samples 1 to 4 for NP (left) and CP4 (right) powders in both longitudinal and transversal sections.

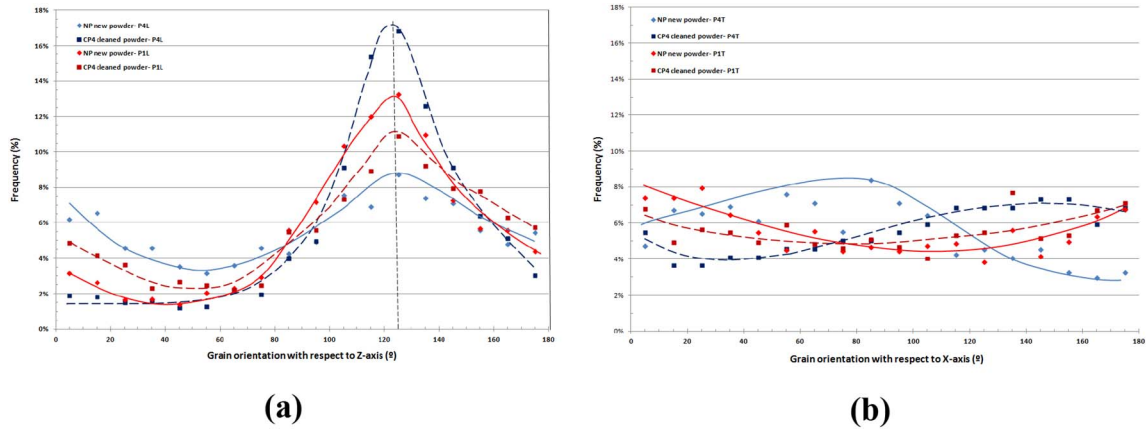


Fig. 10. Grain orientation in the longitudinal (a) and transverse (b) sections of sample 1 (bottom of the build) and 4 (top) from clad builds NP (new powder) and CP4 (4 reuses).

evaluated from optical micrographs using image analysis. The results point out an increase of the porosity with the number of reuses (Fig. 8c). In all the clad builds, porosity is higher at the top of the parts and lower in the middle or the bottom.

The present porosity is spherical which suggests that its origin is due to gas entrapment and the turbulences in the melt pool caused by the interaction between the powder particles and the laser. Excessive superheat increases the fluidity of the molten metal and the extent of gas entrapment in the build. The inter-pass temperature and the time for heat dissipation between passes also concentrate the heat in the melt pool explaining why the porosity is higher in the top of the clad build than in the bottom. Porosity is quasi constant up to the second reuse (CP2) and increases strongly for the 3rd and 4th reuses. The porosity is also slightly higher in the longitudinal than in the transverse direction,

whatever the number of reuses. Strondl [8] and Ardila [11] also pointed out an increase of porosity with the number of builds in the case of SLM.

A more detailed analysis of the microstructure has been made by EBSD (Fig. 9). The grain orientation, size and aspect ratio have been analyzed for the longitudinal as well as the transversal sections for the clad builds processed. For the NP new powder materials, the mean grain size is  $53.4 \mu\text{m}$  with a mean standard deviation of  $35.0 \mu\text{m}$ , for both directions (transverse or longitudinal) and whatever the position (top or bottom). For the CP4 cleaned powder, the mean grain size is  $56.5 \mu\text{m}$  with a mean standard deviation of  $37.2 \mu\text{m}$ , for both directions (transverse or longitudinal) and whatever the position (top or bottom). The grain is slightly larger for the clad build with recycled powder. The tendency is similar for the grain aspect ratio, with values, respectively for NP and CP4 builds, of  $2.10 \pm 1.85$  and  $2.16 \pm 1.66$ , for both

## NP build

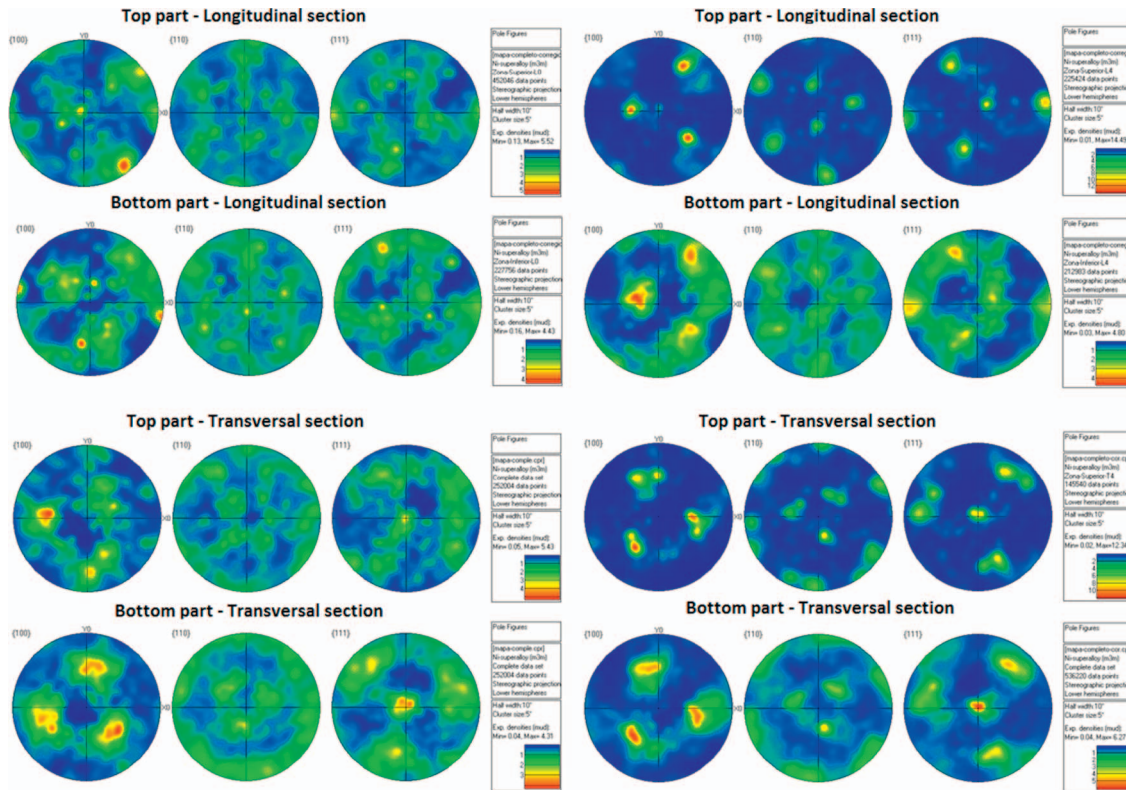


Fig. 11. Pole figures for NP and CP4 clad builds.

directions. The grains are slightly elongated for the build with recycled powder.

For the grain orientation, the conclusions are different (Figs. 10 and 11). For both NP and CP4 clad builds, there is not a preferential orientation of the grains in the X-Y section (Fig. 10b) while for the longitudinal X-Z section the results depend on the sample position in the build and the number of reuses of the powder (Fig. 10a). For samples 1 (bottom of the builds), the microstructure seems to be a mixture of equiaxed and columnar grains but with a strong proportion of columnar grains oriented at  $125^\circ$  with respect to the Z-axis. For sample 4 of the NP build, the microstructure is a mixture of equiaxed and columnar grains but with a slightly orientation at  $125^\circ$ .

Moreover, for the NP clad builds, there is not a particular crystallographic orientation of the grains, while for CP4 clad builds, a  $\langle 111 \rangle$  crystal orientation clearly appears whatever the section (longitudinal or transversal) and the position of the sample (top or bottom) (Figs. 9, 11).

This crystallographic orientation of the grains is more pronounced for sample 4 (top) than for sample 1 (bottom). Even though the solidification rate of this process is quite high as to avoid the formation of laves and delta phase, a network of this brittle phase has been found.

These structures can also be found in wrought alloys after being treated at  $750^\circ\text{C}$  during 100 h [18] but in this case is just the result of the cladding process.

It seems that the thermal cycle generated by the cladding process to add new layers could be the responsible of the apparition of intragranular acicular delta phase (thermodynamically more stable), presumably as transformation of  $\gamma''$  phases during the thermal history. The work carried out by Tian [17] explains with detail the evolution of this microstructure.

Fig. 12a–b shows the micrograph of samples built from new and 4 times reused powders before heat treatment. Both samples exhibit a  $\gamma$  matrix, an acicular and intragranular  $\delta$  phase associated with laves and NbC precipitates. In spite of the similarity of these images, EBDS

analysis and porosity shows differences as already described. The network that can be appreciated in a lighter color corresponds with  $\delta$  phase, laves and niobium carbides, as it can be seen in Fig. 12e.

After thermal treatment (Fig. 12c–d),  $\delta$  phases are solubilized, niobium carbides remain in the  $\gamma$  matrix and niobium distribution improves within the matrix. In the interdendritic area, laves presenting a globular geometry and niobium carbides can be found (Fig. 12f). The comparison between the composition of the phases found in the upper and bottom zones of the block has no shown relevant differences. The laves content has been estimated by image analysis to be around 2%wt., whatever the position in the build or the number of reuses.

#### 3.4. Mechanical Properties

The results of tensile tests are reported in Table 3 and Fig. 13. The characteristics of yield, tensile strengths and Young's modulus are similar to the specifications for IN718 of the AMS 5662M standard whatever the number of recycling or the position of the sample within the clad builds.

In the case of the rupture strain, the values obtained are strongly dependent on the sample position within the build and on the number of reuses of the cleaned powders. The lower is the position of the sample in the build or the higher the number of reuses, the lower the rupture strain. After 2 reuses, the rupture strain also decreases strongly.

#### 4. Interpretations

The different previous results show that the reuse of IN718 powder after the proposed recycling treatment does not modify significantly:

(1) the characteristics of the powders since the chemical composition remains the same, the morphology of the particles evolving towards a distribution of their diameter much centered around an average



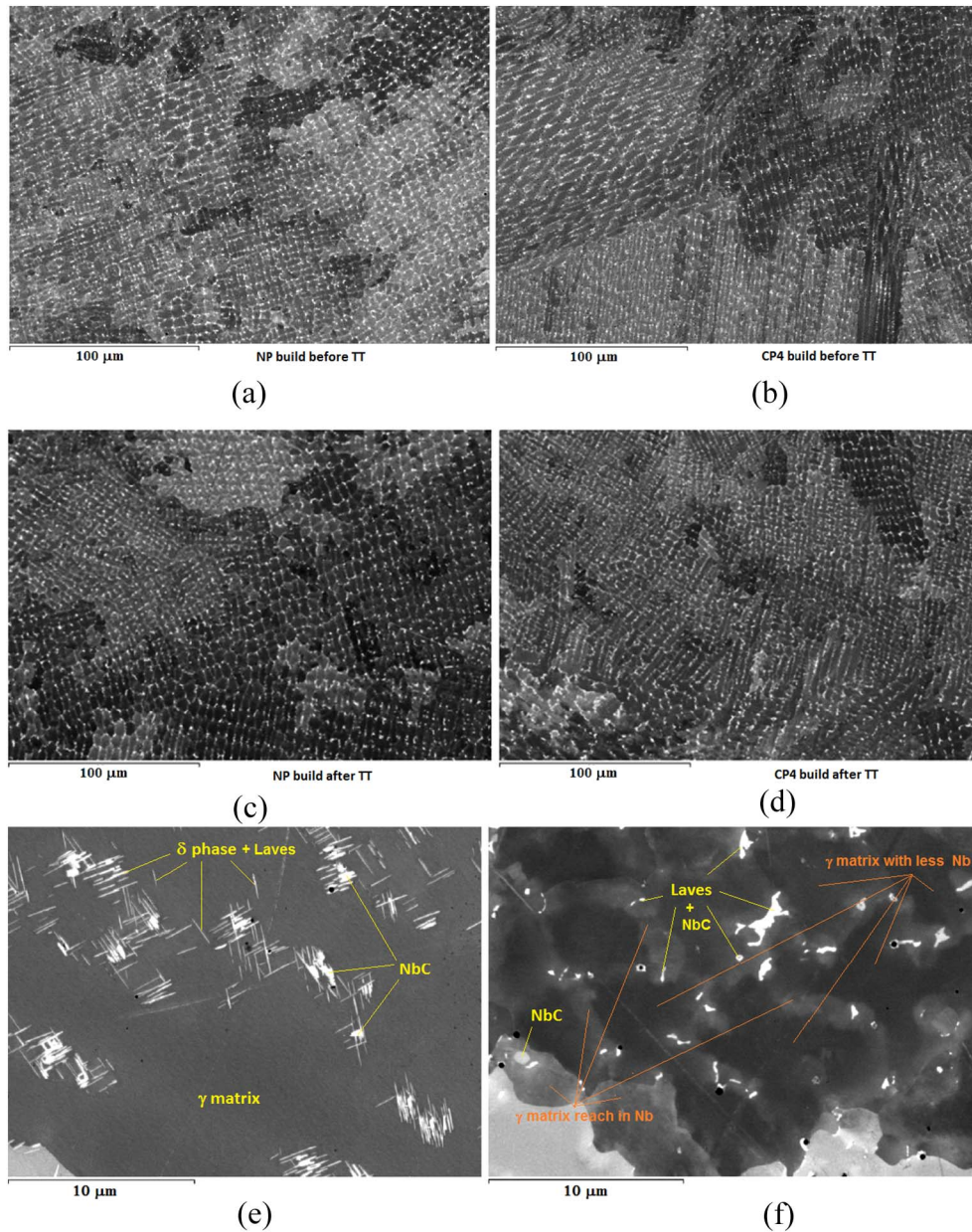


**Fig. 12.** SEM micrographs of NP (a) and CP4 (b) clad builds before and after (c) and (d) heat treatment; SEM micrograph showing the precipitation of brittle delta/laves phases within the matrix (e) before and (f) after heat treatment.

value slightly higher than the initial value, and an aspect ratio value which decreases leading to more spherical particles,

(2) the chemical composition of the clad parts in their thickness, and in function of the number of reuses,

(3) the precipitates content within the height of the build or with the number of reuses,

(4) the yield and rupture strength or the Young's modulus of the fabricated materials.

On the other hand, a drop in the rupture strain was pointed out from a third reuse of the recycled powders. This feature has also been demonstrated in the thickness of the material, the samples in contact with the substrate exhibiting a lower rupture strain than those situated above.

Two phenomena have thus been pointed out concerning the reduction of the rupture strain, (i) one depending on the height of the clad part, and (ii) the other associated with the number of reuse of the powder. The first phenomenon can be attributed to the conditions of implementation of the process and is independent of the quality of the powders and the second to the characteristics evolution of the reused powders.

During the manufacture of the builds on the DIN C45E steel substrate, the thermal conditions of the process evolve over time due to the difference in thermal conductivity and specific heat between the substrate and the deposited material. When the first layers of IN718 are deposited, the heat flow through the substrate is facilitated due to the better thermal conductivity of the steel. When the thickness of the deposit begins to become large, the heat flow is slowed down by the lower thermal conductivity of IN718. This is reflected, as the EBSD analysis shows, by a modification of the microstructure (Fig. 9). In the zone close to the substrate and in the median part, in the longitudinal direction, the grains have a columnar growth with an orientation at  $125^\circ$  with respect to the Z axis, reflecting the presence of a heat flow in the Z direction in addition to the principal one in the Y direction. In the upper part of the build, the solidification becomes predominantly equiaxed with a random orientation of the grains. This evolution has been pointed out by Kirka et al. [19] in the case of the electron beam-melting of IN718. It is also confirmed using the G/R diagram of solidification for IN718 [20] and the model developed by Renderos et al. [21]. Fig. 14 shows

**Table 3**

Mechanical properties of the builds clad with new powder (P0 samples) and recycled powders (P1 to P4 for one to four reuses). Samples referenced PX-1 are located at the bottom of the build and PX-4 at the top.

Sample reference	Rupture strain (%) $\pm$ SD	Young's modulus (GPa) $\pm$ SD	Yield strength (MPa) $\pm$ SD	Tensile strength (MPa) $\pm$ SD
IN718 (AMS 5662M)	12.0		1034.0	1276.0
P0-1	7.6 $\pm$ 3	176.5 $\pm$ 6.3	1209 $\pm$ 46	1368 $\pm$ 39
P0-2	11.2 $\pm$ 3	184.0 $\pm$ 6.3	1235 $\pm$ 46	1403 $\pm$ 39
P0-3	13.8 $\pm$ 3	191.6 $\pm$ 6.3	1271 $\pm$ 46	1451 $\pm$ 39
P0-4	14.0 $\pm$ 3	181.3 $\pm$ 6.3	1162 $\pm$ 46	1372 $\pm$ 39
P1-1	8.8 $\pm$ 3	175.6 $\pm$ 5.1	1202 $\pm$ 19	1368 $\pm$ 31
P1-2	10.1 $\pm$ 3	182.0 $\pm$ 5.1	1226 $\pm$ 19	1401 $\pm$ 31
P1-3	13.2 $\pm$ 3	182.7 $\pm$ 5.1	1241 $\pm$ 19	1430 $\pm$ 31
P1-4	14.5 $\pm$ 3	188.1 $\pm$ 5.1	1244 $\pm$ 19	1435 $\pm$ 31
P2-1	8.8 $\pm$ 3	183.4 $\pm$ 3.1	1222 $\pm$ 17	1388 $\pm$ 29
P2-2	11.1 $\pm$ 3	185.7 $\pm$ 3.1	1257 $\pm$ 17	1450 $\pm$ 29
P2-3	13.5 $\pm$ 3	190.4 $\pm$ 3.1	1256 $\pm$ 17	1448 $\pm$ 29
P2-4	14.6 $\pm$ 3	184.4 $\pm$ 3.1	1236 $\pm$ 17	1428 $\pm$ 29
P3-1	8.0 $\pm$ 2	186.6 $\pm$ 7	1219 $\pm$ 12	1391 $\pm$ 21
P3-2	9.5 $\pm$ 2	172.3 $\pm$ 7	1201 $\pm$ 12	1379 $\pm$ 21
P3-3	9.6 $\pm$ 2	180.0 $\pm$ 7	1210 $\pm$ 12	1388 $\pm$ 21
P3-4	12.0 $\pm$ 2	187.2 $\pm$ 7	1229 $\pm$ 12	1426 $\pm$ 21
P4-1	4.6 $\pm$ 2	184.0 $\pm$ 4.3	1207 $\pm$ 18	1335 $\pm$ 29
P4-3	7.6 $\pm$ 2	192.5 $\pm$ 4.3	1214 $\pm$ 18	1377 $\pm$ 29
P4-4	7.8 $\pm$ 2	189.4 $\pm$ 4.3	1240 $\pm$ 18	1391 $\pm$ 29

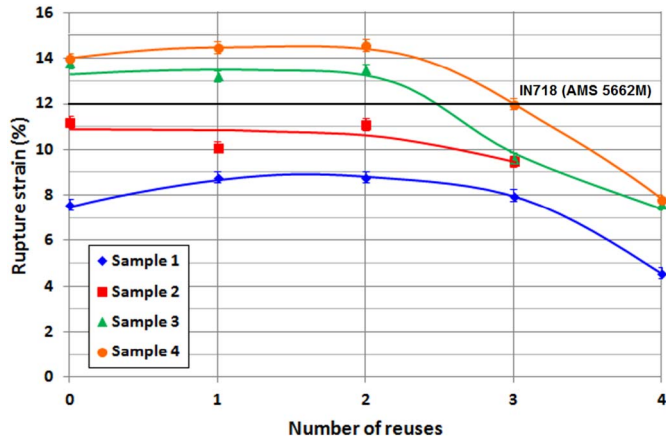


Fig. 13. Evolution of yield strength, ultimate tensile strength and rupture strain as a function of the number of reuses and location of the sample within the clad build.

how the microstructure evolves from a predominantly columnar texture to a mixed columnar/equiaxed one. When the clad is built from the substrate (sample 1 for both cases), the microstructure is columnar at the bottom of the melt pool and mixed or equiaxed at the top. When the different layers are built, this equiaxed zone can be remelted and thus disappear. In the bottom part of the clad (sample 4), the behavior is similar for NP new powder but as the temperature of the substrate has increased the equiaxed microstructure is finer. For CP4 cleaned powder, as the powder diameter is higher, the temperature and the diameter of the melt are higher, resulting in a columnar microstructure and more gas entrapped. Furthermore, the predicted grain sizes are in good agreement with the data of EBDS.

During the tensile tests of samples 1, the loading is carried out in a direction quasi perpendicular to the grains, involving the grain boundaries and the phases present in these zones. This is not the best direction for plastically deforming the material and therefore the

rupture strain is affected. It is therefore quite normal to have an increase in ductility between the bottom and the top of the builds. Li et al. [22] showed, in the case of Ni-Fe alloys, that the strength is independent of grain orientation. However, the plastic strain increased remarkably when the loading axis is parallel to the direction of grain columns, which is due to the enhanced grain boundary and dislocation activities.

When the number of reuses increases, the rupture strain drops rapidly, whatever the position of the samples in the build. This effect is mainly associated with the increase in porosity of the CP3 and CP4 builds. The use of recycled powders with a size distribution highly centered on a higher mean value favors the process stability but also increases the melt temperature [20]. Gas entrapment is favored but also the epitaxy of the solidified microstructure, leading to a columnar microstructure (oriented at 125° with respect to the Z axis), a strong crystallographic orientation ( $\langle 111 \rangle$ ) and a higher porosity.

## 5. Conclusions

In this work it has been observed that the wasted powder of the Laser Material Deposition process maintains morphological and chemical properties after crossing through the nozzle. Some particles react under the influence of the energy source and spinel type oxides appear. However, there are two variables affecting positively the option of recycling the powder: On one hand the scarce amount of non-desirable phases, estimated to be lower than 2% of the recollected powder and, on the other hand the possibility of segregating magnetically these phases from the rest of the powder.

The chemical composition of the recycled powder is similar to the raw material and complies with the standard specifications for the INCO 718 material. Two parameters can limit the reuse of recycled powders: oxygen and niobium content. The recycled powder size distribution is mainly centered on a slightly high mean value.

The builds show no difference in chemical composition or in the different phases depending on the number of reuse. On the other hand, the microstructure evolves towards a columnar structure with a very marked crystallographic orientation ( $\langle 111 \rangle$ ). The static properties of the recycled builds are similar to those of the new powder builds for a limited recycling number (2). Beyond this value, the breaking strain decreases sharply and becomes a limiting factor.

It should be remarked that in this process of reusing the powder, there is no need of adding new material to obtain good quality samples but at the difference with other additive manufacturing processes (EBM or SLM), the reuse of the recycled powder is limited to 2 reuses. The implementation of this step of removing non-desirable phases allows the improvement of the final efficiency, reducing costs and decreasing the hazardous powder amount.

Additional work is currently performed to evaluate the potential of mixing part of the recycled powder with new raw material, and to protect particles from oxidation using a protective gas curtain.

## Acknowledgements

Special thanks are addressed to Inkyu Kim Yun for his work in the experimental part, to the Industry and Competitiveness Spanish Ministry (DPI2013-46164-C2-1-R TURBO project), to the UFI 11/29 in Mechanical Engineering of the UPV/EHU (grant no. 4935/2011) and the Aquitaine-Euskadi Euroregion (PROCECO project) (grant no. 2013/GR1/12) for their financial support. The authors also thank SGIker (Unit of Electron Microscopy and Microanalysis of Materials) of UPV/EHU and European funding (ERDF and ESF) for the technical and human support provided.



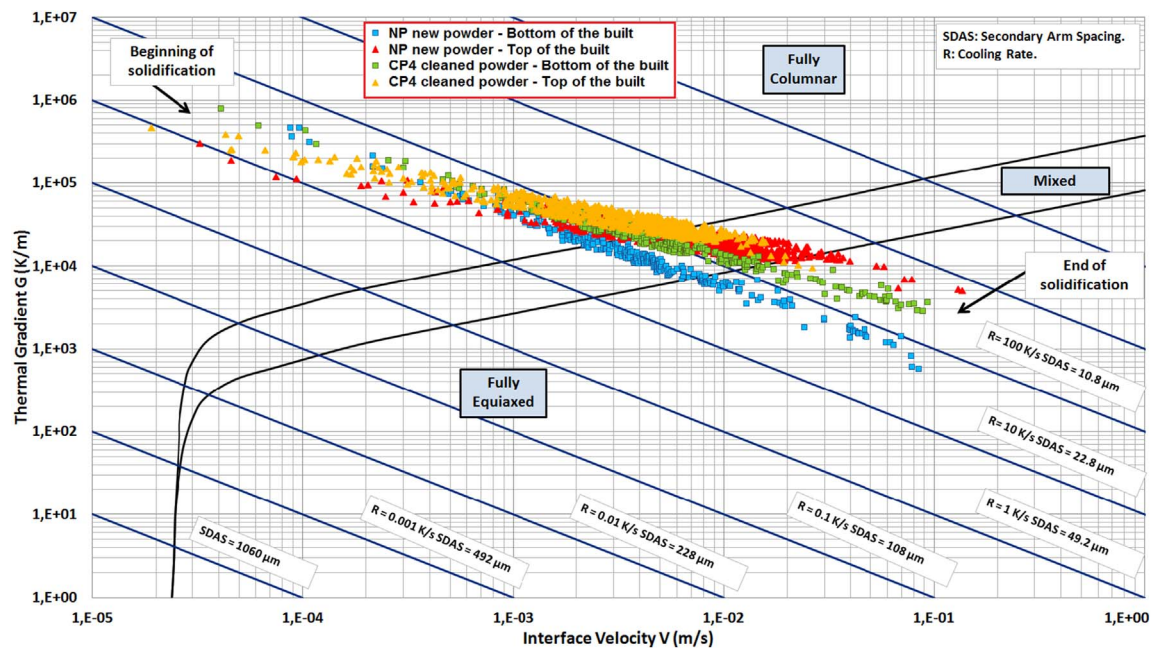


Fig. 14. Solidification map of the different clad blocks for NP and CP4 powders.

## Appendix A. Supplementary data

Supplementary data to this article can be found online at <http://dx.doi.org/10.1016/j.matchar.2017.09.029>

## References

- [1] E. Toyserkani, A. Khajepour, S.F. Corbin, *Laser Cladding*, CRC Press, 2004 (ISBN 9780849321726).
- [2] J.I. Arrizubieta, I. Tabernero, J. Exequiel Ruiz, A. Lamikiz, S. Martínez, E. Ukar, Continuous Coaxial Nozzle Design for LMD Based on Numerical Simulation. *Physics Procedia*, 56 (2014), pp. 429–438, <http://dx.doi.org/10.1016/j.phpro.2014.08.146>.
- [3] J. Cao, L. Fencheng, L. Xin, H. Chunping, C. Jing, H. Weidong, Effect of overlap rate on recrystallization behaviors of Laser Solid Formed Inconel 718 superalloy, *Opt. Laser Technol.* 45 (2013) 228–235, <http://dx.doi.org/10.1016/j.optlaseng.2012.06.043>.
- [4] Z. Liu, H. Qi, Mathematical modeling of crystal growth and microstructure formation in multi-layer and multi-track laser powder deposition of single-crystal superalloy, *Phys. Procedia* 56 (2014) 411–420, <http://dx.doi.org/10.1016/j.phpro.2014.08.144>.
- [5] A.M. Kamara, S. Marimuthu, L. Li, Finite element modeling of microstructure in laser-deposited multiple layer Inconel 718 parts, *Mater. Manuf. Process.* 29/10 (2014) 1245–1252, <http://dx.doi.org/10.1080/10426914.2014.930963>.
- [6] I. Tabernero, A. Lamikiz, S. Martínez, E. Ukar, J. Figueras, Evaluation of the mechanical properties of Inconel 718 components built by laser cladding, *Int J Mach Tool Manu* 51 (6) (2011) 465–470, <http://dx.doi.org/10.1016/j.ijmactools.2011.02.003>.
- [7] J. Lambardi, J. Leunda, V. García Navas, C. Soriano, C. Sanz, Microstructural and tensile characterization of Inconel 718 laser coatings for aeronautic components, *Opt. Lasers Eng.* 51 (2013) 813–821, <http://dx.doi.org/10.1016/j.optlaseng.2013.01.011>.
- [8] A. Strondl, O. Lyckfeldt, H. Brodin, U. Ackelid, Characterization and control of powder properties for additive manufacturing, *J. Miner. Met. Mater. Soc. (TMS)* 67 (3) (2015), <http://dx.doi.org/10.1007/s11837-015-1304-0>.
- [9] V. Petrovic, R. Niñerola, Powder recyclability in Electron Beam Melting for aeronautical use, *Aircr. Eng. Aerosp. Tech.* 87 (2) (2015), <http://dx.doi.org/10.1108/AEAT-11-2013-0212>.
- [10] P. Nandwana, W.H. Peter, R.R. Dehoff, L.E. Lowe, M.M. Kirka, F. Medina, S.S. Babu, Recyclability study on Inconel 718 and Ti-6Al-4V powders for use in electron beam melting, *Metall. Mater. Trans. B* 47B (2016) 754–762, <http://dx.doi.org/10.1007/s11663-015-0477-9>.
- [11] L.C. Ardila, F. Garciandia, J.B. González-Díaz, P. Álvarez, A. Echeverria, M.M. Petite, R. Deffley, J. Ochoa, Effect of IN718 recycled powder reuse on properties of parts manufactured by means of Selective Laser Melting, 8th Int. Conf. on Photonic Technologies LANE 2014, *Phys. Procedia* 56 (2014) 99–107, <http://dx.doi.org/10.1016/j.phpro.2014.08.152>.
- [12] LPW Technologies, Case study 5: powder degradation, (2016) <http://www.lpwtechnology.com/wp-content/uploads/2016/09/LPW-Case-Study-05.pdf>.
- [13] P.A. Carroll, P. Brown, G. Ng, R. Scudamore, A.J. Pinkerton, W. Syed, H. Sezer, L. Li, J. Allen, The effect of powder recycling in direct metal laser deposition on powder and manufactured part characteristics, *Cost Effective Manufacture Via Net-Shape Processing*, Meeting Proceedings RTO-MP-AVT-139, Paper 18. Neuilly-sur-Seine, France: RTO, 2006, pp. 18-1–18-10. Available from: <http://www.rto.nato.int/abstracts.asp>.
- [14] J.A. Slotwinski, E.J. Garboczi, P.E. Stutzman, C.F. Ferraris, S.S. Watson, M.A. Peltz, Characterization of metal powders used for additive manufacturing, *J. Res. Natl. Inst. Stand. Technol.* 119 (2014) 460–493, <http://dx.doi.org/10.6028/jres.119.018>.
- [15] G. Appa Rao, M. Srinivas, D.S. Sarma, Effect of oxygen content of powder on microstructure and mechanical properties of hot isostatically pressed superalloy Inconel 718, *Mater. Sci. Eng. A* 435–436 (2006) 84–99, <http://dx.doi.org/10.1016/j.msea.2006.07.053>.
- [16] J.M. Benson, Safety consideration when handling metal powders, *J. South. Afr. Inst. Min. Metall.* 112 (7) (2012) 563–575 (ISSN: 0038-223X).
- [17] Y. Tian, D. McAllister, H. Colijn, M. Mills, D. Farson, M. Nordin, S. Babu, Rationalization of microstructure heterogeneity in INCONEL 718 builds made by the direct laser additive manufacturing process, *Metall. Mater. Trans. A* 45A (2014) 4470–4483, <http://dx.doi.org/10.1007/s11661-014-2370-6>.
- [18] M.G. Burke, M.K. Miller, Precipitation in alloy 718: a combined AEM and APFIM investigation, in: E.A. Loria (Ed.), *Proc. Superalloys 718, 625 and Various Derivatives*, June 1991, Pittsburgh, PA, The Minerals, Metals and Materials Society, Warrendale, PA, 1991, pp. 337–350.
- [19] M.M. Kirka, F. Medinac, R. Dehoffa, A. Okello, Mechanical behavior of post-processed Inconel 718 manufactured through the electron beam melting process, *Mater. Sci. Eng. A* 680 (2017) 338–346, <http://dx.doi.org/10.1016/j.addma.2016.09.001>.
- [20] M.M. Kirka, K.A. Unocic, N. Raghavan, F. Medina, R.R. Dehoff, S.S. Babu, Microstructure development in electron beam-melted Inconel 718 and associated tensile properties, *JOM* 68 (3) (2016), <http://dx.doi.org/10.1007/s11837-016-1812-6>.
- [21] M. Renderos, F. Girot, E. Lacoste, Determination of G/R Maps for Microstructure Prediction, Internal Report for AENIGME Joint Transborder Laboratory, University of the Basque Country (UPV/EHU), University of Bordeaux (UBx) and ENSAM, 2016-01.
- [22] H. Li, P.K. Liaw, H. Choo, A. Misra, Effect of grain orientation on ductility in a nanocrystalline Ni-Fe alloy, *Appl. Phys. Lett.* 93 (2008) 051907, <http://dx.doi.org/10.1063/1.2968662>.